

Direction dependent B-splines decomposition for the registration of sliding objects

Vivien Delmon, Simon Rit, Romulo Pinho, David Sarrut

CREATIS, CNRS UMR 5220, Inserm U1044, INSA-Lyon, University of Lyon,
F-69621 Villeurbanne, France

Léon Bérard Cancer Center, University of Lyon, F-69373 Lyon, France
vivien.delmon@creatis.insa-lyon.fr

Abstract. Sliding motion is a difficult issue in regularised deformable image registration. A typical example occurs in thoracic 4D CT images where the lungs slide along the ribcage. Current solutions use a prior segmentation which separates the image into different regions with the sliding at the interface and register each region separately. However, this can lead to physically implausible deformations at the interface. In this paper, we locally separate the motion in the normal direction to handle it with a single B-spline transformation on the whole image, defining a motion field which varies continuously. The rest of the deformation is separately handled in each label by a B-spline transformation allowing discontinuity at interfaces. We compared our approach to prior solutions and obtained similar target registration errors with more physically plausible deformation.

1 Introduction

The measurement of breathing motion is required in many applications, e.g., the 4D radiotherapy of thoracic and upper-abdominal tumors. Motion estimation is generally done between different phases of a 4D CT using deformable registration.

Deformable registration is an ill-posed problem which requires regularization to obtain smooth vector fields. However, true anatomical motion can be locally non-smooth. This is the case at the pleura, where the lung slides along the ribcage. Global regularizations would enforce smoothness everywhere, although the result should display singularities at sliding locations.

Several approaches have been proposed to handle this problem. In [10,16], an adapted regularization is used to preserve sliding motion. These regularizations are based on the intensities of the CT image, making them sensitive to noise and inadequate where the intensities are similar on both sides of the sliding, e.g., in the upper abdomen. In [9], the regularization is expressed on the deformation field to penalize physically implausible deformations while allowing sliding. In [3,15,17], a segmentation is used to limit the motion estimation to a region, e.g. the lungs, the rest of the thoracic region being separately registered. This solution allows discontinuity along the interface and preserves smoothness elsewhere

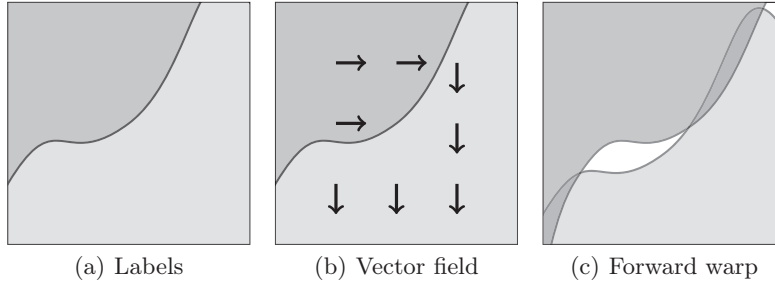


Fig. 1. Gaps (white) or overlaps (dark gray) can appear with one B-spline per label.

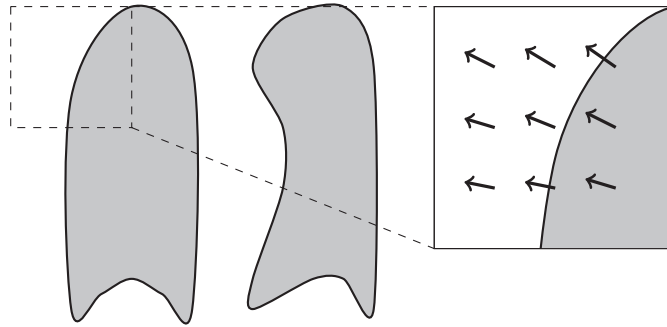


Fig. 2. Normal vector field \mathbf{N} .

(Figure 1(b)). However, two independent registrations are likely to produce inconsistent motion estimates, resulting in gaps and overlaps at the interface of the forward warp (Figure 1(c)). To handle this, [14,17] modified voxel intensity values around the segmented region to constrain the deformation field. This solution forces the segmentation to be done on both the fixed and the moving image increasing the impact of a bad or inconsistent segmentation.

Moreover, although sliding motion implies a discontinuity at the interface, it is smooth in the direction normal to the interface, called $\mathbf{N} : \mathbb{R}^3 \rightarrow \mathbb{R}^3$ in the following (Figure 2). This observation has lead Schmidt-Richberg *et al.* to constrain diffusive registration by regularizing the motion field in the \mathbf{N} directions [13].

In this paper, we describe the motion parallel to this normal direction using a B-spline deformable registration [12], which is among the most popular methods for lung registration [7]. During registration, we locally decompose the transformations according to the normal direction to form a single B-spline transformation constrained to vary in the normal direction and one B-spline transformation for each region handling the rest of the motion, thus allowing discontinuity at the interface between regions in the direction parallel to the interface. By separating the motion in the normal direction and handling it with a B-spline transform, we force it to be continuous at any point.

2 Method

2.1 Motion mask segmentation

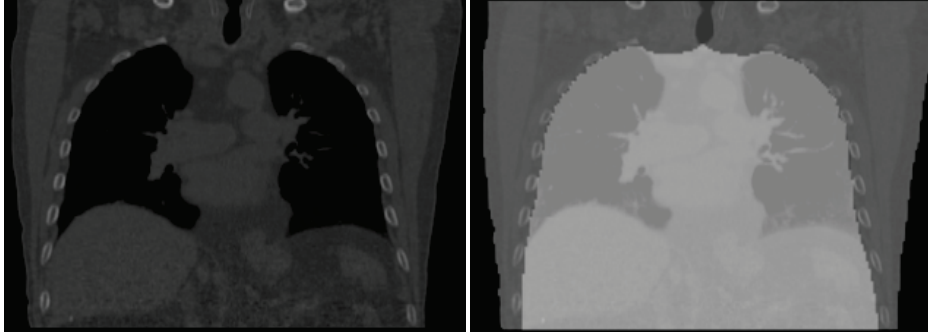


Fig. 3. Left: coronal slice of a 4D CT. Right: Corresponding motion mask segmentation.

The patient is segmented, following the suggestion of Wu *et al.* [17] (Figure 3). The segmented *motion mask* $\Omega \subset \mathbb{R}^3$ encompasses the organs with the largest displacements during breathing, comprising the lung, the mediastinum and the abdomen; the complementary region $\bar{\Omega}$ encompasses the more static organs, comprising the thoracic cage and the backbone. Automated segmentation is achieved using the method described in [14], which is based on level-sets constrained by pre-segmented anatomical features, mainly the lungs and the bones. The objective of this study is to improve the accuracy of the registration by accounting for sliding motion at the border of Ω .

2.2 B-splines for sliding motion

As in previous works, we use one B-spline transformation per region Ω and $\bar{\Omega}$ to allow discontinuity of the estimated motion at the interface. However, the local deformation in the direction \mathbf{N} is separated in an additional B-spline transformation which covers the entire image. Thus, potential inconsistencies between the deformations in Ω and $\bar{\Omega}$ are prevented because deformation is smooth in the direction \mathbf{N} , while sliding is possible because the remaining deformations are handled by the other two independent B-spline transformations.

Formally, let $\mathbf{B}^{\mathbf{N}}, \mathbf{B}^{\Omega}, \mathbf{B}^{\bar{\Omega}} : \mathbb{R}^3 \rightarrow \mathbb{R}^3$ be three B-spline continuous deformations representing the deformation in the \mathbf{N} directions, orthogonal to \mathbf{N} in Ω and orthogonal to \mathbf{N} in $\bar{\Omega}$, respectively. All three deformations were defined on the same set of knot points with their respective B-spline coefficients $\mathbf{c}_i^{\mathbf{N}}, \mathbf{c}_i^{\Omega}, \mathbf{c}_i^{\bar{\Omega}} \in \mathbb{R}^3$, e.g.,

$$\mathbf{B}^{\mathbf{N}}(\mathbf{x}) = \sum_{i \in J} \mathbf{c}_i^{\mathbf{N}} \beta_i(\mathbf{x})$$

with \mathbf{x} in \mathbb{R}^3 , $\mathbf{i} \in \mathbf{J} \subset \mathbb{Z}^3$ the spatial indices of the B-spline knots and $\beta_{\mathbf{i}}$ the tensor product of one-dimensional B-spline kernels, $\beta_{\mathbf{i}} = \prod_j \beta_{\mathbf{i}}^j$. The sought deformation $\mathbf{T} : \mathbb{R}^3 \rightarrow \mathbb{R}^3$ is defined as

$$\mathbf{T}(\mathbf{x}) = \begin{cases} \mathbf{B}^{\mathbf{N}}(\mathbf{x}) + \mathbf{B}^{\Omega}(\mathbf{x}) & \text{if } \mathbf{x} \in \Omega, \\ \mathbf{B}^{\mathbf{N}}(\mathbf{x}) + \mathbf{B}^{\overline{\Omega}}(\mathbf{x}) & \text{if } \mathbf{x} \in \overline{\Omega}. \end{cases} \quad (1)$$

During registration, the three B-spline transformations are constrained to vary in fixed directions to respect their definitions: collinear to \mathbf{N} for $\mathbf{B}^{\mathbf{N}}$ and orthogonal to \mathbf{N} for \mathbf{B}^{Ω} and $\mathbf{B}^{\overline{\Omega}}$. First, $\mathbf{B}^{\mathbf{N}}$ is set in the direction of \mathbf{N} at any point of space by constraining the motion of each B-spline knot in the \mathbf{N} directions at its location with

$$\mathbf{c}_{\mathbf{i}}^{\mathbf{N}} = p_{\mathbf{i}}^{\mathbf{N}} \mathbf{N}(\mathbf{i}) \quad (2)$$

where $p_{\mathbf{i}}^{\mathbf{N}} \in \mathbb{R}$ is a single parameter for the knot \mathbf{i} of $\mathbf{B}^{\mathbf{N}}$ defining the amount of its motion along $\mathbf{N}(\mathbf{i})$. The collinearity of \mathbf{N} and $\mathbf{B}^{\mathbf{N}}$ is not strictly enforced but it will be very close to the normal if \mathbf{N} is locally smooth, which is a reasonable assumption [13].

Then, \mathbf{B}^{Ω} and $\mathbf{B}^{\overline{\Omega}}$ must be orthogonal to \mathbf{N} at any point in space. We compute two vector fields $\mathbf{U}, \mathbf{V} : \mathbb{R}^3 \rightarrow \mathbb{R}^3$ so that $\{\mathbf{N}(\mathbf{x}), \mathbf{U}(\mathbf{x}), \mathbf{V}(\mathbf{x})\}$ forms a local base at any point $\mathbf{x} \in \mathbb{R}^3$. $\mathbf{U}(\mathbf{x})$ and $\mathbf{V}(\mathbf{x})$ can be any basis in the plane defined by $\mathbf{N}(\mathbf{x})$. We compute $\mathbf{U}(\mathbf{x})$ with the cross products between $\mathbf{N}(\mathbf{x})$ and the unit vector of the image basis corresponding to the smallest component of $\mathbf{N}(\mathbf{x})$ to ensure numerical stability. $\mathbf{V}(\mathbf{x})$ is deduced with the cross product of $\mathbf{N}(\mathbf{x})$ and $\mathbf{U}(\mathbf{x})$. The motion of each B-spline knot of \mathbf{B}^{Ω} and $\mathbf{B}^{\overline{\Omega}}$ is constrained in a direction orthogonal to \mathbf{N} with

$$\begin{aligned} \mathbf{c}_{\mathbf{i}}^{\Omega} &= p_{\mathbf{i}}^{\Omega, \mathbf{U}} \mathbf{U}(\mathbf{i}) + p_{\mathbf{i}}^{\Omega, \mathbf{V}} \mathbf{V}(\mathbf{i}) \\ \mathbf{c}_{\mathbf{i}}^{\overline{\Omega}} &= p_{\mathbf{i}}^{\overline{\Omega}, \mathbf{U}} \mathbf{U}(\mathbf{i}) + p_{\mathbf{i}}^{\overline{\Omega}, \mathbf{V}} \mathbf{V}(\mathbf{i}) \end{aligned} \quad (3)$$

where $p_{\mathbf{i}}^{\Omega, \mathbf{U}}, p_{\mathbf{i}}^{\Omega, \mathbf{V}}, p_{\mathbf{i}}^{\overline{\Omega}, \mathbf{U}}, p_{\mathbf{i}}^{\overline{\Omega}, \mathbf{V}} \in \mathbb{R}$ are two pairs of parameters constraining \mathbf{B}^{Ω} and $\mathbf{B}^{\overline{\Omega}}$ respectively.

Solving the registration problem with sliding motion comes down to estimating the optimal parameters $p_{\mathbf{i}}^{\mathbf{N}}, p_{\mathbf{i}}^{\Omega, \mathbf{U}}, p_{\mathbf{i}}^{\Omega, \mathbf{V}}, p_{\mathbf{i}}^{\overline{\Omega}, \mathbf{U}}$, and $p_{\mathbf{i}}^{\overline{\Omega}, \mathbf{V}}$ in the sense of a chosen similarity measure to characterize the three constrained B-spline transformations. Subsequently, the final transformation \mathbf{T} can be derived from equations 1, 2, and 3.

2.3 Partial derivatives

Several optimization processes use a matrix of partial derivatives of the output components of the transformation with respect to the parameters. Since we use a linear combination of B-spline transformations in each region, we obtain a B-spline transformation per region with conventional properties (separable,

derivable, ...). Therefore, we can derive partial derivatives of the transformation by combining the ones of each underlying B-spline transformation. The combination is achieved by projecting the derivatives on \mathbf{N} , \mathbf{U} , and \mathbf{V} :

$$\frac{\partial_{\mathbf{x}} \mathbf{T}(\mathbf{x})}{\partial_{p_i^N}} = \frac{\partial_{\mathbf{x}} \mathbf{B}^N(\mathbf{x})}{\partial_{c_{i,x}^N}} \times \mathbf{N}(\mathbf{x}) \qquad \frac{\partial_{\mathbf{x}} \mathbf{T}(\mathbf{x})}{\partial_{p_i^{\Omega,U}}} = \frac{\partial_{\mathbf{x}} \mathbf{B}^{\Omega}(\mathbf{x})}{\partial_{c_{i,x}^{\Omega}}} \times \mathbf{U}(\mathbf{x}).$$

3 Implementation and Evaluation

3.1 Implementation

Our implementation is based on elastix, which is a toolbox for intensity-based medical image registration [4]. Elastix is based on the ITK registration framework and extends it with, e.g., spatial regularization. The elastix framework allows users to add their own components and to use them in combination with other components.

We implemented a new transformation component which takes a segmented image as a parameter. The vector field \mathbf{N} is derived from this segmentation by computing the normal on the interface and propagating it to the whole image using an isotropic propagation. From \mathbf{N} , we deduce \mathbf{U} and \mathbf{V} to instantiate the three B-splines. The rest of the component dispatches transformation methods (partial derivatives, point transformation, ...) on these B-splines.

We wrote an elastix wrapper allowing us to use our new component with other elastix components (optimizers, metrics, samplers, ...). We used the recommended optimizer, metric and image sampler, i.e., the Adaptive Stochastic Gradient Descent and a random sampler [5] and the Mattes Mutual Information [6].

3.2 Results

Patients The method was applied to the exhale and inhale frames of 4D CT images of the thorax of 16 lung cancer patients.

The first 6 patients were part of a radiotherapy planning protocol. The images were acquired on a Brilliance Big Bore 16-slice CT scanner (Philips Medical Systems, Cleveland, OH). Retrospective respiratory-correlated reconstruction into ten 3D CT images was made possible by simultaneous recording of a respiratory trace using the Pneumo Chest bellows (Lafayette Instrument, Lafayette, IN). The original resolution was approximately $1 \times 1 \times 2$ mm. All images were resampled to a 2 mm isotropic voxel prior to processing, resulting in a typical size of $256 \times 256 \times 150$ voxels. All patients had 100 landmarks manually selected by physicians on exhale and inhale frames.

The 10 following patients are from the dir-labs (DL) database which is freely available at <http://www.dir-labs.com>. The original resolution of these images was $0.97 \times 0.97 \times 2.5$ with about $512 \times 512 \times 128$ voxels, the five first were cropped around the ribcage and then resampled to have about $256 \times 256 \times 100$ voxels

Patient	Before			Single region			Multi regions			Multi regions with normal		
	Mean	SD	Max	Mean	SD	Max	Mean	SD	Max	Mean	SD	Max
1	9.36	7.42	32.1	2.74	3.4	16.1	1.25	1.04	7.26	1.28	1.06	7.37
2	7.33	4.86	24.1	2.44	2.95	19.2	1.52	1.86	14.7	1.59	1.95	14.7
3	7.09	5.08	19.8	2.31	2.49	14.7	1.28	0.842	5.43	1.31	0.857	5.23
4	6.68	3.67	14.2	1.92	2.09	10.4	0.963	0.54	3.55	0.985	0.563	3.84
5	14	7.17	32.4	5.36	5.5	23.3	1.41	0.983	6.69	1.58	1.17	7.08
6	5.73	2.6	14	1.37	0.966	4.56	1.17	0.635	3.6	1.22	0.757	4.33
DL 1	3.89	2.78	10.9	1.51	1	6.47	1.11	0.498	2.66	1.13	0.514	2.82
DL 2	4.34	3.9	17.7	1.85	1.88	11.8	1.02	0.485	2.95	1.05	0.505	3.05
DL 3	6.94	4.05	16.6	3.21	2.36	12.9	1.49	0.773	5.51	1.79	1.02	6.16
DL 4	9.83	4.85	20.3	3.21	2.7	14.5	1.59	1.07	11.4	1.62	1.08	11.6
DL 5	7.48	5.5	24.8	4	3.72	15.8	1.83	1.51	15.8	1.87	1.55	16
DL 6	10.9	6.96	27.6	5.05	4.24	22.9	1.62	0.923	5.4	1.74	1.03	5.48
DL 7	11	7.42	30.6	6.97	6.14	26.8	1.74	1.04	6.39	2.1	1.34	7.37
DL 8	15	9	30.6	10.9	9.92	32.7	1.69	1.53	14.5	2.34	2.33	17
DL 9	7.92	3.97	15.8	4.27	2.86	13.5	1.53	0.816	4.68	1.65	0.95	5.41
DL 10	7.3	6.34	27.8	3.93	4.5	24.6	1.6	1.26	9.74	1.64	1.3	9.69
average	8.42	5.64	22.45	3.82	4.15	16.89	1.42	1.05	7.51	1.55	1.21	7.94

Table 1. Target Registration Error after 3 resolutions (in mm).

slightly changing the resolution, the five others were not cropped and kept their original size and resolution. Each dir-labs patient has 300 landmarks on exhale and inhale frames. The protocol used to obtain these landmarks is described in [2] for the 5 first patients and in [1] for the others.

Protocol We used third order B-spline transformations with 32 mm between knot points in all directions. The Mattes Mutual Information metric used 2048 voxels randomly chosen at each iteration. The moving image was interpolated using third order B-splines. To take into account large deformations, we used a multi resolution strategy by smoothing the image with a Gaussian kernel. Results presented in Table 1 were obtained after 3 resolutions of 4000 iterations each, using a 2.8 GHz single-thread processor. The multi regions methods took around 7 minutes and 45 seconds and the multi regions with normal took around 9 minutes. This difference comes from some fixed costs like the normal vector field computation at the beginning, the local base computation at each resolution, and from costs involved at each iteration such as the parameters dispatch between each underlying B-spline transform.

Results Compared to a single B-spline transformation, the use of a multi-regions registration reduced the average target registration error from 3.82 mm to 1.42 mm by allowing non-smooth motion on interfaces (Figure 4). The method

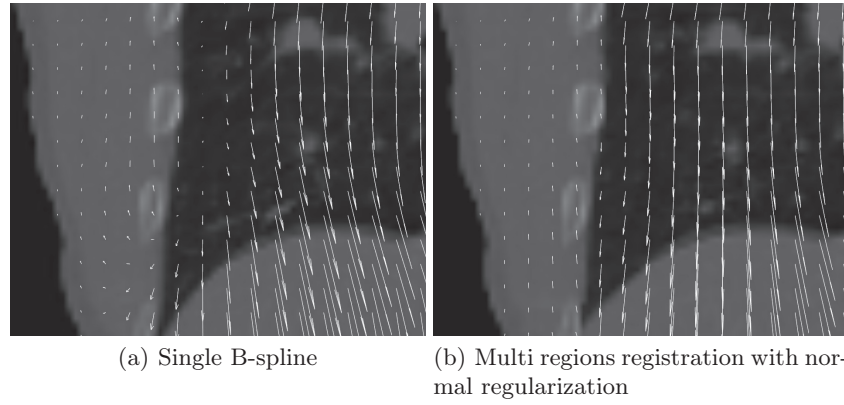


Fig. 4. Deformation vector fields. (sampled each 4mm)

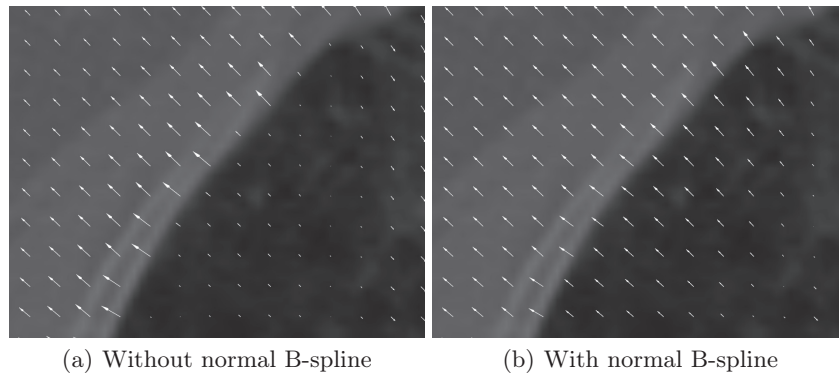


Fig. 5. Projection of the normal component of the deformations obtained with the two multi region algorithms. (sampled each 4mm)

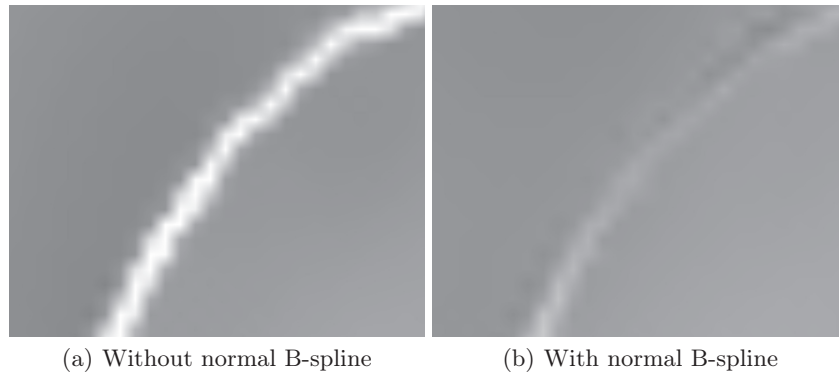


Fig. 6. The quality measure associated with Figure 5. (grey is better)

presented in this study kept the target registration error low (1.55 mm) and ensured a better smoothness of the deformation vector field in the normal direction, producing more realistic results (Figure 5). These results are close to the best registered dir-labs results. Our mean registration error for dir-labs results is 1.52 mm for the multi-regions approach and 1.69 mm for the multi-regions with normal approach where best dir-labs results are 1.44 mm and 1.25 mm [1]. The second model the 4D local trajectory using all phases of the 4DCT to obtain such good results.

The regularity of a deformation field can be measured using the determinant of the Jacobian of this deformation [8]. A Jacobian between 0 and 1 represents a local expansion and a Jacobian superior to 1 a local shrinkage. We used a logarithm to project these values on $] - \infty, +\infty[$ (Figure 6) and took the mean of the absolute value around the motion mask border to quantify the gain of the separated normal B-spline transform. The quality measure

$$\frac{1}{N_x} \sum_x |\log(|Jac(proj(T(x), \mathbf{N}))|)|$$

applied to our patient databases gave the results listed in Table 2 and showed a better smoothness of the normal part of the deformation vector field with our method.

Patient	Multi regions	Multi regions with normal
1	0.206	0.165
2	0.162	0.124
3	0.168	0.123
4	0.197	0.170
5	0.328	0.215
6	0.198	0.122
DL 1	0.103	0.090
DL 2	0.135	0.116
DL 3	0.218	0.123
DL 4	0.180	0.128
DL 5	0.179	0.137
DL 6	0.318	0.204
DL 7	0.285	0.189
DL 8	0.378	0.284
DL 9	0.234	0.179
DL 10	0.224	0.164
average	0.220	0.159

Table 2. Smoothness measure of the normal part of the deformation field around the sliding interface.

4 Discussion and Conclusion

We presented a method to model the physiology of sliding motion using B-spline transformations. This model was achieved by separating the motion component collinear to the normal field from the rest of the motion and treating it on the whole image. The tangential component was treated independently in each region allowing discontinuity at the interface for this direction only.

Our method can be extended to handle more regions. For instance, one region per organ can model a body in which organs are allowed to slide along each other. The proposed method is also backward compatible with our previous workflow based on two independent registrations. Since the normal is only required during registration, the final result can be expressed using one B-spline per label by reintroducing the normal coefficients.

Compared to the use of two registrations, i.e., one per label, the proposed method has less parameters per control point around the interface (five instead of six), showing the restricted degrees of freedom in this area. With two registrations, there are three parameters for each label overlapping around the interface, whereas our method requires two parameters for each label plus one for the common normal.

Methods that compute one registration per label also change voxel values around the segmentation to constrain interfaces to match [14,17]. However, these methods must segment both the moving and the fixed image, and the segmentation must be consistent between these images. In case of inconsistency, it forces the mapping of both borders which do not represent the same physical region. Our method, on the other hand, requires the segmentation of the fixed image only, and the impact of a bad segmentation is less important since it only affects the representation of the sliding motion in the mis-segmented part of the image.

In this work, the normal regularization relies on the intrinsic B-spline smoothness, which depends on the knot spacing. If one increases the number of knot points, the smoothness will be insufficient. It remains possible to use additional regularizations expressed on the spatial derivatives of the underlying B-splines. However, regularizations expressed directly on B-spline coefficients, such as diffeomorphic regularization [11], will be investigated because the direction of each B-spline with respect to \mathbf{N} must be enforced during registration.

Acknowledgments

This work was supported in part by Association Nationale de la Recherche Technique (ANRT) and in part by Elekta Oncology Systems.

References

1. Castillo, E., Castillo, R., Martinez, J., Shenoy, M., Guerrero, T.: Four-dimensional deformable image registration using trajectory modeling. *Physics in Medicine and Biology* 55(1), 305 (2010), <http://stacks.iop.org/0031-9155/55/i=1/a=018>

2. Castillo, R., Castillo, E., Guerra, R., Johnson, V.E., McPhail, T., Garg, A.K., Guerrero, T.: A framework for evaluation of deformable image registration spatial accuracy using large landmark point sets. *Physics in Medicine and Biology* 54(7), 1849 (2009), <http://stacks.iop.org/0031-9155/54/i=7/a=001>
3. Kabus, S., Klinder, T., Murphy, K., van Ginneken, B., Lorenz, C., Pluim, J.P.W.: Evaluation of 4D-CT lung registration. In: *Medical Image Computing and Computer-Assisted Intervention – MICCAI 2009*. pp. 747–754 (2009)
4. Klein, S., Staring, M., Murphy, K., Viergever, M., Pluim, J.: elastix: a toolbox for intensity-based medical image registration. *IEEE Trans Med Imaging* 29(1), 196–205 (Jan 2010), <http://dx.doi.org/10.1109/TMI.2009.2035616>
5. Klein, S., Pluim, J., Staring, M., Viergever, M.: Adaptive stochastic gradient descent optimisation for image registration. *International Journal of Computer Vision* 81, 227–239 (2009), <http://dx.doi.org/10.1007/s11263-008-0168-y>
6. Mattes, D., Haynor, D., Vesselle, H., Lewellen, T., Eubank, W.: PET-CT image registration in the chest using free-form deformations. *IEEE Trans Med Imag* 22(1), 120–128 (2003)
7. Murphy, K., van Ginneken, B., Reinhardt, J., Kabus, S., Ding, K., Deng, X., Pluim, J.: Evaluation of Methods for Pulmonary Image Registration: The EMPIRE10 Study. In: *Medical Image Analysis for the Clinic: A Grand Challenge*. pp. 11–22 (2010)
8. Rey, D., Subsol, G., Delingette, H., Ayache, N.: Automatic detection and segmentation of evolving processes in 3D medical images: Application to multiple sclerosis. *Med Image Anal* 6(2), 163–179 (Jun 2002)
9. Ruan, D., Esedoglu, S., Fessler, J.A.: Discriminative sliding preserving regularization in medical image registration. In: *Proceedings of the Sixth IEEE international conference on Symposium on Biomedical Imaging: From Nano to Macro*. pp. 430–433. ISBI'09, IEEE Press, Piscataway, NJ, USA (2009), <http://portal.acm.org/citation.cfm?id=1699872.1699981>
10. Ruan, D., Fessler, J.A., Esedo, S.: Discontinuity preserving regularization for modeling sliding effects in medical image registration. In: *Proc. IEEE Nuc. Sci. Symp. Med. Im. Conf.*, pp. 5304-8 (2008)
11. Rueckert, D., Aljabar, P., Heckemann, R., Hajnal, J., Hammers, A.: Diffeomorphic registration using B-splines. *Med Image Comput Comput Assist Interv* 9(Pt 2), 702–709 (2006)
12. Rueckert, D., Sonoda, L., Hayes, C., Hill, D., Leach, M., Hawkes, D.: Nonrigid registration using free-form deformations: application to breast MR images. *IEEE Trans Med Imaging* 18(8), 712–721 (Aug 1999), <http://dx.doi.org/10.1109/42.796284>
13. Schmidt-Richberg, A., Ehrhardt, J., Werner, R., Handels, H.: Slipping objects in image registration: improved motion field estimation with direction-dependent regularization. *Med Image Comput Comput Assist Interv* 12(Pt 1), 755–762 (2009)
14. Vandemeulebroucke, J., Bernard, O., Kybic, J., Clarysse, P., Sarrut, D.: Automatic motion mask extraction for deformable registration of the lungs. In: *XVIth International Conference on the Use of Computers in Radiation Therapy*. Amsterdam (June 2010)
15. Werner, R., Ehrhardt, J., Schmidt-Richberg, A., Handels, H.: Validation and comparison of a biophysical modeling approach and non-linear registration for estimation of lung motion fields in thoracic 4D CT data. In: *Proceedings of SPIE- The International Society for Optical Engineering*. vol. 7259 (Februari 2009)

16. Wolthaus, J., Sonke, J.J., van Herk, M., Damen, E.: Reconstruction of a time-averaged midposition CT scan for radiotherapy planning of lung cancer patients using deformable registration. *Med Phys* 35(9), 3998–4011 (2008)
17. Wu, Z., Rietzel, E., Boldea, V., Sarrut, D., Sharp, G.: Evaluation of deformable registration of patient lung 4DCT with subanatomical region segmentations. *Med Phys* 35(2), 775–781 (Feb 2008)